AGU100 ADVANCING EARTH AND SPACE SCIENCE

Space Weather

RESEARCH ARTICLE

10.1029/2018SW001843

Special Section:
Space Weather Capabilities Assessment

Analytical Representations for Characterizing the Global Aviation Radiation Environment Based on Model and Measurement Databases

W. Kent Tobiska[1,2], Leonid Didkovsky[1], Kevin Judge[1], Seth Weiman[1], Dave Bouwer[1], Justin Bailey[1], Bill Atwell[1], Molly Maskrey[1], Chris Mertens[3], Yihua Zheng[4], Margaret Shea[5], Don Smart[5], Brad Gersey[1,6], Richard Wilkins[6], Duane Bell[6], Larry Gardner[7], and Robert Fuschino[8]

[1]Space Weather Division, Space Environment Technologies, Los Angeles, CA, USA, [2]Now at Space Environment Technologies, Los Angeles, CA, USA, [3]Space Radiation Group, NASA Langley Research Center, Hampton, VA, USA, [4]Community Coordinated Modeling Center, NASA Goddard Space Flight Center, Greenbelt, MD, USA, [5]SSSRC, Nashua, NH, USA, [6]Department of Electrical Engineering, Prairie View A. & M. University, Prairie View, TX, USA, [7]Department of Physics, Utah State University, Logan, UT, USA, [8]FPS, Highlands Ranch, CO, USA

Key Points:
- Analytical functions have been constructed that represent the NAIRAS model and ARMAS measurement databases of the radiation environment
- These functions enable global climatological and statistical weather forecasting of aviation radiation hazards
- These functions represent the GCR radiation component and the GCR plus probable REP radiation components

Supporting Information:
- Supporting Information S1

Correspondence to:
W. K. Tobiska,
ktobiska@spacenvironment.net

Citation:
Tobiska, W. K., Didkovsky, L., Judge, K., Weiman, S., Bouwer, D., Bailey, J., et al. (2018). Analytical representations for characterizing the global aviation radiation environment based on model and measurement databases. *Space Weather*, *16*. https://doi.org/10.1029/2018SW001843

Received 23 FEB 2018
Accepted 7 SEP 2018
Accepted article online 16 SEP 2018

Abstract The *Nowcast of Atmospheric Ionizing Radiation for Aviation Safety* climatological model and the *Automated Radiation Measurements for Aerospace Safety* (ARMAS) statistical database are presented as polynomial fit equations. Using equations based on altitude, *L* shell, and geomagnetic conditions an effective dose rate for any location from a galactic cosmic ray (GCR) environment can be calculated. A subset of the ARMAS database is represented by a second polynomial fit equation for the GCR plus probable relativistic energetic particle (REP; Van Allen belt REP) effective dose rates within a narrow band of *L* shells with altitudinal and geomagnetic dependency. Solar energetic particle events are not considered in this study since our databases do not contain these events. This work supports a suggestion that there may be a REP contribution having an effect at aviation altitudes. The ARMAS database is rich in Western Hemisphere observations for *L* shells between 1.5 and 5; there have been many cases of enhanced radiation events possibly related to effects from radiation belt particles. Our work identifies that the combined effects of an enhanced radiation environment in this *L* shell range are typically 15% higher than the GCR background. We also identify applications for the equations representing the Nowcast of Atmospheric Ionizing Radiation for Aviation Safety and ARMAS databases. They include (i) effective dose rate climatology in comparison with measured weather variability and (ii) climatological and statistical weather nowcasting and forecasting. These databases may especially help predict the radiation environment for regional air traffic management, for airport overflight operations, and for air carrier route operations of individual aircraft.

Plain Language Summary Analytical functions have been constructed that represent the Nowcast of Atmospheric Ionizing Radiation for Aviation Safety model and Automated Radiation Measurements for Aerospace Safety measurement databases of the radiation environment at commercial aviation altitudes; the functions enable global climatological and statistical weather nowcasting and forecasting of aviation radiation hazards during quiet to active geomagnetic conditions.

1. Background

1.1. The Radiation Environment

Two major sources of radiation hazards have been known for decades, that is, galactic cosmic rays (GCRs) and solar energetic particles (SEPs). GCRs are produced in the galaxy outside the solar system in high-energy supernova explosive events and consist mostly of energetic protons that, when they penetrate the heliosphere, are slowly modulated by the strength of the Sun's interplanetary magnetic field (Simpson, 1983). SEPs come from solar activity such as coronal mass ejections related to flaring events or from interplanetary magnetic field shocks (Gopalswamy, 2004; Reames, 2013). In the latter case fast coronal mass ejections plow through a slower solar wind creating a shock front to produce accelerated energetic protons. Recently, a third radiation source has been suggested that could originate from relativistic energetic particle (REP) precipitation from the Van Allen radiation belts. This effect has been called a radiation cloud although a more physical perspective is flight through a γ ray beam.

Whatever their source, these charged particles are constrained to spiral around Earth's magnetic field lines and the centroid of motion along the particle trajectory forms an adiabatic invariant that is characterized as the McIlwain *L* shell (McIlwain, 1961). The McIlwain *L* parameter is a useful proxy for magnetic latitude and geomagnetic cutoff rigidity (Smart & Shea, 1967) and also accounts for the evolution of changes in the Earth's magnetic field (Shea et al., 1987). GCRs and SEPs can reach any magnetic latitude depending upon their energy. Radiation belt particles are constrained to enter the Earth's atmosphere along a narrow band defined by McIlwain *L* shells between 2 and 7. Dachev et al. (2017) have called these precipitation bands. Only the highest-energy particles (usually protons or heavy ions) are found in equatorial and low latitudes while even low-energy particles (including many electrons) enter the atmosphere at high latitudes. Because there are additional lower-energy particles (greater flux), the result is a higher radiation environment at higher magnetic latitudes. As the Earth's magnetospheric magnetic field dynamically changes due to perturbations from the solar wind, the *L* shells will dynamically intersect different geographic latitudes in each hemisphere.

Charged particles such as protons (p^+), electrons (e^-), alpha particles (α), and heavier ions up to iron such as Fe^{26+} entering the top of the atmosphere are the primary radiation field. Below the terrestrial atmosphere's mesopause near 85 km, the incident particles begin colliding with ambient N_2 and O_2 to create a spray of secondary and tertiary particles as well as photons. These include neutrons (n), p^+, e^-, α, pions (π), muons (μ), γ rays, and X-rays with each having lower energy than the primary particle. As the primary particles are increasingly absorbed at lower altitudes, they compete in ionization with the increasing secondary and tertiary population that is simultaneously produced. This can result in a maximum ionization rate between 20 and 25 km (65,000–82,000 ft) called the Regener-Pfotzer maximum (Carlson & Watson, 2014; Regener & Pfotzer, 1935). Below this altitude down to the Earth's surface, the dose rate from all radiation decreases due to particle and photon absorption in an increasingly thick atmosphere. These secondary and tertiary particles and photons collide with an aircraft hull and its interior components (people, materials, and fuel) to further alter the radiation spectrum that is then deposited in tissue (International Agency for Research on Cancer, 2000; Tobiska et al., 2017; United Nations Scientific Committee on the Effect of Atomic Radiation (UNSCEAR), 2000) and avionics (Mutuel, 2016; Normand et al., 1994, 2006).

1.2. Aviation Safety Concerns Related to Human Tissue

Tobiska et al. (2017) summarize the safety concerns of radiation for aviation. In human tissue, radiation can cause atoms and molecules to become ionized, dissociated, or excited. These processes occur through (i) production of free radicals, (ii) breakage of chemical bonds, (iii) production of new chemical bonds and cross-linkage between macromolecules, and (iv) damage of molecules that regulate vital cell processes, such as deoxyribonucleic acid, ribonucleic acid, and proteins (UNSCEAR, 2000). High linear energy transfer (LET, a measure of energy lost by a radiation per unit track length) radiations (neutrons, alpha particles, and heavier ions) are generally more harmful to living tissues per unit dose (energy deposited per unit of target mass) than low-LET radiations (photons, muons, and electrons). Protons and charged pions are considered low-LET radiation but interact like high-LET radiations often enough to be treated separately in dosimetry (ICRP, 2007). While cell death can occur across a range of dose levels, at high doses an organ's cell population can drop so rapidly that cells cannot be replaced quickly enough resulting in the tissue failing to function normally (International Agency for Research on Cancer, 2000; UNSCEAR, 2000). This is not the case with the dose levels achieved during most aviation experiences, and instead, epidemiological studies in occupational groups associated with aviation have been conducted for several decades focussing on radiation-associated cancer; there continues to be broad discussion in this field of study (e.g., Grajewski et al., 2011).

1.3. Aviation Safety Concerns Related to Avionics

In addition to potential health effects including an increased lifetime cancer risk, Tobiska et al. (2017) summarize damage to avionics that might endanger flight safety. A broad community has studied this topic in detail (e.g., Dyer & Lei, 2001; Dyer et al., 2003a; Dyer & Truscott, 1999; Mutuel, 2016; Normand et al., 1994, 2006). Other bodies have investigated the avionics safety issue extensively, including the International Commission on Radiation Units (ICRU) Joint Report (84), the International Electrotechnical Commission Single Event Effects (SEE) standard for avionics (International Electrotechnical Commission 62396–1, 2012), the Joint Electron Device Engineering Council Solid State Technology Association SEE standard for avionics (JESD89A), the World Meteorological Organization observing requirements (#709, #738), and the

International Civil Aviation Organization regulatory guidelines (Standards and Recommended Practices 3.8.1). A further discussion is beyond the scope of this paper.

1.4. Previous Studies Relevant to This Study

There have been a number of campaign and flight databases created over the past few decades that capture a wide range of dosimetric measurements. Aircraft (Dyer et al., 2009, 2003a, 2003b, 2005; Federico et al., 2015; Getley et al., 2010; Iles et al., 2004; Lee et al., 2015; Meier et al., 2009; Meier, Matthiä, et al., 2016; Meier, Trompier, et al., 2016; Ploc et al., 2013), balloon (Mertens, 2016; Mertens et al., 2016), and ISS (Dachev, 2017; Dachev et al., 2015, 2017) measurements have provided valuable information.

An extensive aircraft radiation measurement database has been compiled using the Liulin instrument (Ploc et al., 2011; Spurny & Dachev, 2002) on commercial aircraft (Ploc et al., 2013). A long-term database of radiation measurements onboard Czech Airlines aircraft since 2001 has been created with many flights between Prague and New York as well as Prague and South America. The database contains dependencies on flight altitude, geographical position, and solar activity. In fact, these measurements convincingly demonstrate three phenomena: (i) the solar cycle effect upon GCR-induced radiation at aviation altitudes where higher dose rates are seen during solar cycle 23 minimum conditions, (ii) geomagnetic field shielding via cutoff rigidities for low versus high geomagnetic latitude flights, and (iii) the ability to capture ground-level events with a continuously monitoring system using the example of ground-level event 60 occurring on 15 April 2001 (Spurny & Dachev, 2001). The *Automated Radiation Measurements for Aerospace Safety* (ARMAS) data discussed below in this study reinforce and expand item (ii).

Several groups have conducted cross-calibration flights with different instruments aboard aircraft. Meier et al. (2009) have provided a systematic overview of dosimetry at aviation altitudes, including the Concorde (Meier, Trompier, et al., 2016). Tissue equivalent proportional counters (TEPCs) have been flown with a QinetiQ QDOS/Rayhound spectrometer, the Liulin 4SA, the Eberline FH 41B, and neutron-sensitive bubble detectors (Dyer et al., 2009; Getley et al., 2010) on Boeing 747-400 Qantas Airways flights covering the Northern and Southern Hemispheres (August 2008 to March 2009). These high northern and southern latitudes as well as cross-equatorial flights demonstrated that spectrometers can provide reliable dose assessments for real-time, in-flight aircrew monitoring and provide timely alerts for solar particle events. Lee et al. (2015) also used the Liulin detector to measure the dose rate environment over the Korean peninsula on military aircraft at a constant altitude of 9 km during geomagnetically quiet to slightly disturbed conditions ($0 \leq Kp \leq 4$) during the decline of solar cycle 24. Both the Liulin and Rayhound detectors compared favorably with the TEPC and were within the generally accepted tolerance of 20% (Dyer et al., 2009).

Flights during solar particle events are rare. However, a sampling of data has been collected for Concorde flights during 29 September 1989 and 19–24 October 1989 (Dyer et al., 2003a, 2003b) as well as the 14 July 2000, 15 April 2001, 29 October 2003, and 20 January 2005 events (Dyer et al., 2005; Iles et al., 2004) using the Cosmic Radiation Effects and Activation Monitor instrument where calculations for the latter event show that dose rates can be elevated several hundred folds for a short duration of time. Additionally, aircraft flights measuring dose rates under the South Atlantic Anomaly (SAA) are also sparse. Federico et al. (2015) have reported measurements in this region along the Brazilian coast onboard military aircraft from December 2010 to June 2011 at altitudes between 4 and 13 km during quiet and low geomagnetic conditions ($0 \leq Kp \leq 3$). They concluded that there is no influence from the SAA protons on the radiation dose at flight altitudes during calm solar and magnetospheric conditions. The ARMAS data do not contain measurements during SEP events.

The National Aeronautics and Space Administration (NASA) *Radiation Experiment* (RaD-X) balloon and aircraft campaign (Mertens, 2016; Meier, Matthiä, et al., 2016) collected dosimetric measurements at seven altitudes from 8 to 32 km over 18 hr near Fort Sumner, New Mexico, during solar and geomagnetically quiet conditions. The measurements focused on regions starting at commercial aviation altitudes and extending beyond the Regener-Pfotzer maximum. The measurements were taken at similar cutoff rigidities, which enabled the dosimetric statistical uncertainty to be reduced below 5%. The campaign found that between 21- and 27-km protons comprise the dominant contribution from cosmic ray primaries (Norman et al., 2016), while at altitudes $>$32 km cosmic ray heavy-ion primaries are discernible. ARMAS data were first validated with the RaD-X measurements (Tobiska et al., 2016).

The low Earth orbital (LEO) environment is essentially the top-of-the-atmosphere boundary condition. While many measurements and studies have investigated the LEO radiation environment, of particular interest is the database created from instruments on the International Space Station (ISS) including the Liulin instrument. Dachev et al. (2015) summarize the most significant results obtained in space and on aircraft, balloon, and rocket flights since 1989. The ISS Liulin measurements (Dachev, 2017; Dachev et al., 2017) identified four source categories: (i) GCR particles and their secondary products, (ii) protons in the SAA region of the inner radiation belt, (iii) relativistic electrons and/or bremsstrahlung in the outer radiation belt (ORB), and (iv) SEP events. Radiation phenomena at aviation altitudes that are possibly a result of relativistic electrons in LEO (Blake et al., 1996) have been suggested by Tobiska et al. (2016), and an in-depth study would be useful to compare ISS Liulin and ARMAS data for the same locations and times.

1.5. Metrics and Baseline Development Motivation for the Study

There is a broad regulatory and ICRP recommendations context that drives international interest in monitoring the aviation radiation environment. We have previously discussed this framework for international and U. S. national levels in detail (Tobiska et al., 2015). It is partly from this perspective that the U.S. government Executive Branch has been interested in developing metrics and baselines related to the effect of space weather on its critical infrastructure. The *Space Weather Strategy and Action Plan* (SWAP; National Science and Technology Council, 2015) and the Presidential Executive Order Coordinating Efforts to Prepare the Nation for Space Weather Events (Executive Order 13744, 2016) both support the development and validation of an operational radiation monitoring and forecasting capability related to space weather. In particular, SWAP seeks to (i) define the requirements for real-time monitoring of the charged particle radiation environment to protect the health and safety of crew and passengers during space weather events; (ii) define the scope and requirements for a real-time reporting system that conveys situational awareness of the radiation environment to orbital, suborbital, and commercial aviation users during space weather events; and (iii) develop or improve models for the real-time assessment of radiation levels at commercial flight altitudes. Summaries of the community's work in this area for extreme events include Tobiska et al. (2017) and Morley et al. (2018). Tobiska et al. (2016) describe how the ARMAS program supports the measurement (monitoring), reporting (situational awareness), and modeling (specification and forecasting) thrusts of the SWAP and Executive Order (EO) 13744 initiatives. In this paper we provide our first functional baselines based on observations and modeling for calculating the ionizing radiation environment relevant to commercial aviation.

2. ARMAS Observations

2.1. ARMAS Program

Tobiska et al. (2015, 2016) described the evolution of the ARMAS program. The goal of ARMAS is to build, demonstrate, and deploy a system that includes a fleet of radiation measurement flight units making real-time dose measurements, an ability to retrieve those data, and immediately process them into tissue-relevant dose rates for use by end users. A fleet of instruments that can operationally monitor radiation in aircraft, balloons, rockets, reusable launch vehicles, and satellites can enable real-time identification of radiation hazards during space weather events, including those from solar protons and radiation belt charged particles during geomagnetically disturbed conditions.

2.2. ARMAS Instrumentation

The ARMAS instruments use Teledyne micro dosimeters, which directly measure total ionizing dose absorbed by a Silicon test mass. By accurately measuring the energy absorbed from heavy ions, alphas, protons, neutrons, electrons, and γ rays, a calibrated measurement of the absorbed dose in Silicon, D (Si), can be made. In addition to the micro dosimeter and a microprocessor there are a variety of data transmission methods (Iridium, Bluetooth, and Ethernet) to report real-time dose rates from vehicles during flight. Once the data are on the ground, D (Si) is converted to equivalent dose, ambient dose equivalent, and effective dose rates. This TRL 9 system has flown since 2013 on flights including NASA Armstrong Flight Research Center's DC-8, ER-2 and G-III, National Oceanic and Atmospheric Administration's (NOAA) G-IV, National Science Foundation/National Center for Atmospheric Research's G-V, and Federal Aviation Agency's Bombardier Global 5000. It has also flown commercially and on a World View Enterprises Stratollite high-altitude balloon.

There are seven generations of the ARMAS Flight Module now being used (Tobiska et al., 2016) with nearly a dozen instruments.

2.3. ARMAS Database

The ARMAS program has created a database of measurements for characterizing the radiation environment around Earth at aviation altitudes. This database reflects dose relevant to GCRs and probably REPs; we have not yet observed SEPs. ARMAS Flight Modules have obtained 411,429 1-min radiation measurements from the ground to 35 km through 553 aircraft and balloon flights (http://sol.spacenvironment.net/armas_ops/Archive/). ARMAS data are now being used in the NASA RADIAN project for data simulation into the NASA Langley Research Center's *Nowcast of Atmospheric Ionizing Radiation for Aviation Safety* (NAIRAS) model. NAIRAS (v1) produces data-driven, physics-based climatology of time-averaged global radiation conditions (Mertens et al., 2013). It covers the entire domain of interest using physics-based modeling and predicts dosimetric quantities from the surface of the Earth, through the atmosphere, and into LEO from both GCRs and SEPs. It includes the response of the geomagnetic field to interplanetary dynamical processes and subsequent influences on atmospheric dose. It uses coupled physics-based models to transport cosmic radiation through three distinct domains: the heliosphere, Earth's magnetosphere, and neutral atmosphere. The physics-based models are driven by real-time measurements to specify boundary conditions on the cosmic and solar radiation at the interfaces between the distinct domains or to characterize a domain's internal properties through which radiation propagates. Since SEPs have been rare, NAIRAS provides an excellent data-driven climatological estimate of GCR-induced radiation. Through RADIAN ARMAS real-time data will be used with NAIRAS to nowcast radiation weather.

The measurement database discussed below captures part of the dynamic variability of radiation weather. Analytical functions using altitude levels in 1-km steps between 8 and 19 km, geomagnetic activity (NOAA G-scales), and McIlwain *L* shell values to represent the effective dose rate have been derived from the ARMAS-absorbed dose in Silicon (Tobiska et al., 2016) measurements. Figure 1 shows the ARMAS measurement database of 1-min flight data records processed with the ARMAS (v9.41) algorithms (Tobiska et al., 2016). The 1-min records contain both unique flight conditions as well as external space environment parameters of interest.

Each flight file contains metadata identifying the start and end dates/times, duration, instrument source, general environmental conditions, flight dosimetric information, measurement uncertainty, and programmatic information. Each 1-min record contains date and time, longitude, latitude, altitude, levels 1–4 doses and dose rates, cutoff rigidity, quality factor, geomagnetic latitude and longitude, McIlwain *L* shell, and other space weather information. Tobiska et al. (2016) describe the derivation and calibration of the ARMAS measurements by comparison with the RaD-X experiment, including the determination of the 24% total uncertainty that is dominated by the mostly GCR-induced radiation. This is less than the ICRU criterion of 30% uncertainty for dose assessments (ICRU, 2010).

In order to further understand uncertainty in the ARMAS data, we have independently compared it with TEPC measurements on two recent flights. Table 1 provides a summary of those results with the average TEPC values and the range of 1-min variability for ARMAS. In general, we find that ARMAS reports lower flight total absorbed dose (Si) compared to TEPC simply because the micro dosimeter is not sensitive to low dose rates at altitudes under 26,000 ft., that is, during ascent to cruise altitude and descent to landing. While the ARMAS-absorbed dose rate (Si) at cruise altitude is very similar to TEPC, the dose equivalent rate at cruise altitude is lower for ARMAS. This is likely because the quality factor used by ARMAS is an analytic function determined by vertical cutoff rigidity (Tobiska et al., 2016) and not a function of ionizing radiation type, for example, neutron, proton, γ ray, as TEPC is able to determine. The statistics of two flights are not enough to make a formal error analysis compared to the work done in the RaD-X campaign (Tobiska et al., 2016), but the similarity between ARMAS and TEPC for the fundamental measurement of absorbed dose rate (Si) at cruise altitude gives us further confidence in the quality of the ARMAS data set. In Table 1, we also show comparative NAIRAS results.

Figure 2 is a horizontal slice of Figure 1 at 11 km where the ARMAS effective dose rate, dE/dt or $\dot{E}$, 1-min weather data records are compared with NAIRAS GCR climatology for G0 geomagnetic conditions. The corresponding *D*-index is also shown. The 1-min radiation weather data records are overlaid onto the climatology map. The full set of figures shown as Figures S2a–S2x in the supporting information provides altitude layers between 9 and 14 km by geographic latitude and longitude and under NOAA G-scale geomagnetic

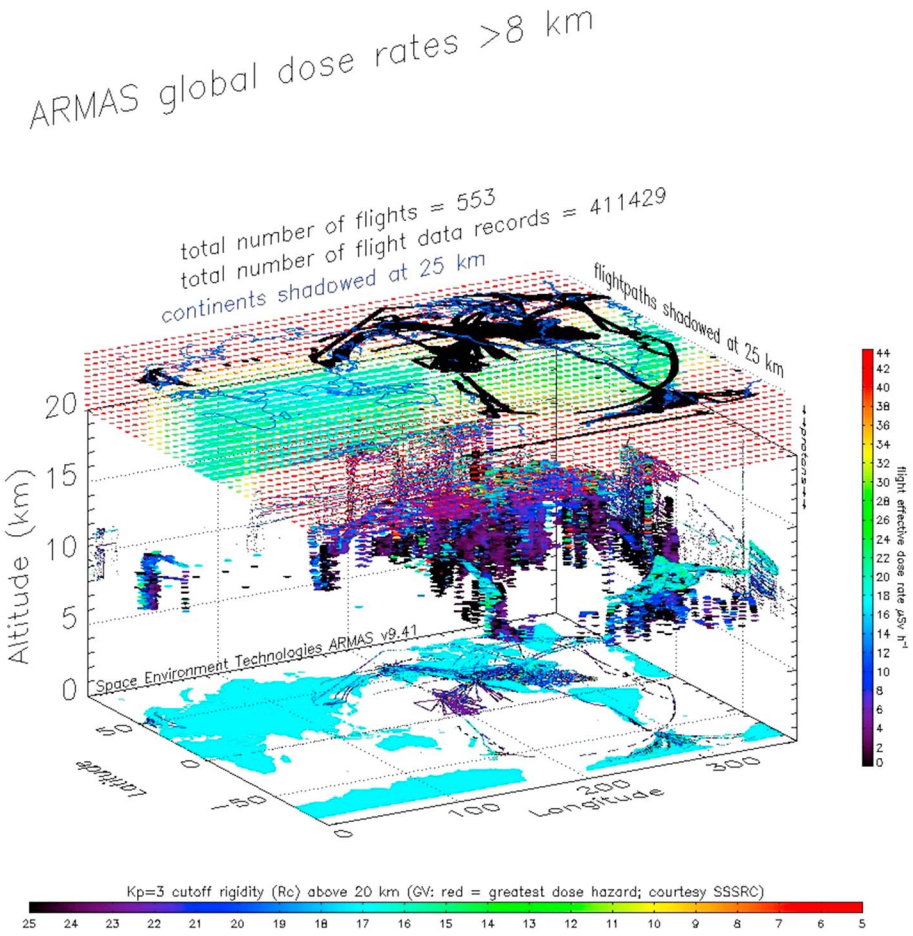

Figure 1. Global ARMAS dose rates above 8 km for all geomagnetic conditions. ARMAS = Automated Radiation Measurements for Aerospace Safety.

conditions from G0 to G3. The *D*-index is calculated from equation (1) and is slightly modified from the original formulation (Meier & Matthiae, 2014; Tobiska et al., 2017) where it now includes all radiation sources. The *D*-index covers a wide range of radiation exposure at aviation altitudes using small natural numbers in a base 2 calculation related to tissue relevant effective dose rates, $\dot{E}$ (μSv/hr). It is defined as the smallest natural number, including zero, to satisfy the inequality:

$$\dot{E} < 5 \times 2^{D} \tag{1}$$

Table 1
TEPC, ARMAS, and NAIRAS Flight Comparisons

Database	Flight start/end	Flight date/ time (UT)	Flight total absorbed dose (Si; μGy)	Absorbed dose rate at cruise (μGy/hr)	Flight total dose equivalent (μSv)	Flight dose equivalent rate at cruise (μSv/hr)	Average quality factor at cruise (unitless)
TEPC (HAWK)	LAX-DEN	20-5-2018/15:35	3.35	2.37	6.65	4.69	1.9
ARMAS v9.41	LAX-DEN	20-5-2018/15:35	2.80–2.94	1.26–2.94	6.67	2.86–6.67	2.0–2.1
NAIRAS v1	LAX-DEN	20-5-2018/15:35		1.16–1.57		3.14–7.33	
TEPC (HAWK)	DEN-LAX	23-5-2018/00:00	3.93	2.51	8.59	5.48	2.12
ARMAS v9.41	DEN-LAX	23-5-2018/00:00	1.96–2.10	1.26–2.10	4.90	2.94–4.90	2.0–2.1
NAIRAS v1	DEN-LAX	23-5-2018/00:00		1.17–1.65		2.09–5.24	

Note. TEPC = tissue equivalent proportional counter; ARMAS = Automated Radiation Measurements for Aerospace Safety; NAIRAS = Nowcast of Atmospheric Ionizing Radiation for Aviation Safety; UT = universal time.

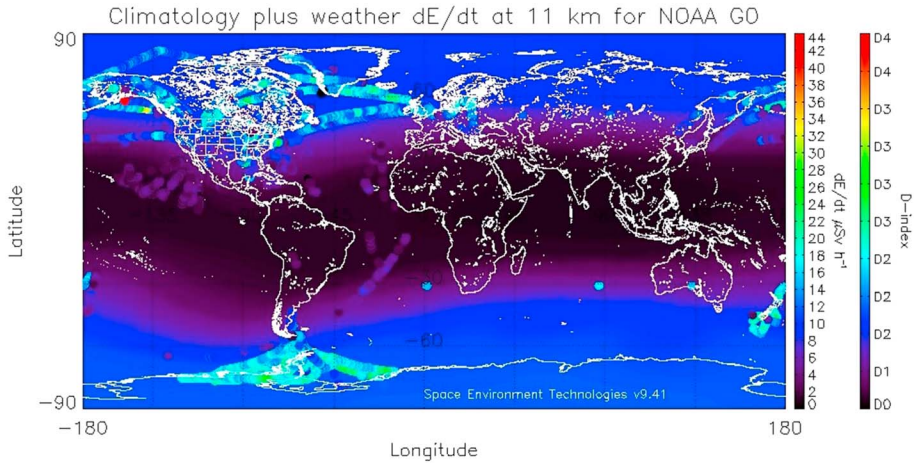

Figure 2. Nowcast of Atmospheric Ionizing Radiation for Aviation Safety galactic cosmic ray background climatology for NOAA G0 geomagnetic conditions at 11 km with Automated Radiation Measurements for Aerospace Safety weather data overlaid. NOAA = National Oceanic and Atmospheric Administration.

The *D*-indices range from *D*0 to *D*8. Quiet conditions are *D*0, *D*1, or *D*2 levels. The *D*3 level (>20 μSv/hr), for example, indicates an elevated radiation intensity that can be used by air traffic management to trigger a radiation alert within the framework of already existing warning systems.

2.4. GCR Analytical Function

We have derived a set of analytical function coefficients in Table 2 that, when used in equation (2), represent NAIRAS climatological and ARMAS median statistical weather effective dose rates for higher LET sources. An example is shown in Figure 3 (and supporting information Figures S3a–S3x). Equation (2) generates the effective dose rate, $\dot{E}$, in μSv/hr as a function of the McIlwain L shell (between $1.5 \le L \le 10$), the NOAA G-scale geomagnetic conditions (between G0 and G3), and altitude ($9 \le z \le 14$ km). Equation (2) represents only the GCR component of the radiation environment at aviation altitudes and excludes contributions from either SEPs or REPs. It is a ninth degree polynomial fit to the databases and is given as follows:

$$\dot{E}(L)_{z,GX} = A_0 + A_1 L + A_2 L^2 + A_3 L^3 + A_4 L^4 + A_5 L^5 + A_6 L^6 + A_7 L^7 + A_8 L^8 + A_9 L^9 \quad (2)$$

2.5. REP Analytical Function

While the ARMAS database is still sparse in several regions (Eastern Hemisphere, altitudes >13 km, G3 or greater geomagnetic conditions, and $L > 5$), we have identified a subset of eight cases that represent the combined GCR + probable REP median value effective dose rate for NOAA G0 and G1 geomagnetic conditions and altitudes of 9, 10, 11, 12 and 13 km for $1.5 \le L \le 5$. In Figure 4 (and Figures 4a–4d in the supporting information) we show an example of an effective dose rate versus L shell at a constant altitude and G0 geomagnetic conditions. There were no SEPs during these flights. The heavy black and red lines through the ARMAS data are the mean and median polynomial fits, respectively, that show the effect of lower LET bremsstrahlung radiation possibly from primary source REPs combined with the slowly varying higher LET GCR-induced background radiation component during 2013–2018. This is from solar cycle 24 decline to solar minimum. The heavy blue line in Figure 4 is the ARMAS GCR background alone listed in Table 2 and also plotted as a solid blue line in Figure 3. The polynomial fit to the median GCR *plus* REP data yields equation (3) for an enhanced effective dose rate, $\dot{E}$, (μSv/hr). The median value coefficients for the eight cases are listed in Table 3 and can be used in equation (3), which is the second degree polynomial fit:

$$\dot{E}\,(L)_{z,GX} = B_0 + B_1 L + B_2 L^2 \quad (3)$$

Table 2
Effective Dose Rate Coefficients for GCRs From NAIRAS and ARMAS Databases

Database	*z*, *GX*	A_0	A_1	A_2	A_3	A_4	A_5	A_6	A_7	A_8	A_9
NAIRAS	09, G0	−0.26853	−19.2052	37.0138	−24.3229	8.49878	−1.77694	0.230066	−0.01811	0.000796	−1.5E-05
ARMAS	09, G0	−6.66914	8.21397	−1.79960	0.610343	−0.13397	−0.01392	0.010674	−0.00174	0.000122	−3.3E-06
NAIRAS	10, G0	11.3435	−50.0061	69.2196	−41.5165	13.9147	−2.84465	0.363541	−0.02840	0.001243	−2.3E-05
ARMAS	10, G0	−5.66914	8.21397	−1.79960	0.610343	−0.13397	−0.01392	0.010674	−0.00174	0.000122	−3.3E-06
NAIRAS	11, G0	35.5295	−110.184	129.619	−73.4335	23.9811	−4.84018	0.614669	−0.04789	0.002093	−3.9E-05
ARMAS	11, G0	−4.66914	8.21397	−1.79960	0.610343	−0.13397	−0.01392	0.010674	−0.00174	0.000122	−3.3E-06
NAIRAS	12, G0	53.1448	−154.760	174.962	−97.5821	31.6570	−6.37556	0.809825	−0.06319	0.002768	−5.2E-05
ARMAS	12, G0	−3.66914	8.21397	−1.79959	0.610342	−0.13397	−0.01392	0.010674	−0.00174	0.000122	−3.3E-06
NAIRAS	13, G0	77.5801	−209.252	224.611	−121.798	38.8060	−7.71772	0.971336	−0.07527	0.003279	−6.1E-05
ARMAS	13, G0	−2.66914	8.21397	−1.79960	0.610343	−0.13397	−0.01392	0.010674	−0.00174	0.000122	−3.3E-06
NAIRAS	14, G0	98.3892	−254.849	265.037	−140.810	44.1943	−8.68757	1.08328	−0.08331	0.003607	−6.7E-05
ARMAS	14, G0	−1.66914	8.21397	−1.79959	0.610343	−0.13397	−0.01392	0.010674	−0.00174	0.000122	−3.3E-06
NAIRAS	09, G1	−45.4098	79.2008	−52.6103	20.5664	−5.17704	0.866581	−0.09619	0.006816	−0.00027	5.04E-06
ARMAS	09, G1	−0.78372	4.35865	0.336721	−1.13914	0.779416	−0.27476	0.053265	−0.00574	0.000324	−7.5E-06
NAIRAS	10, G1	−36.7119	54.8246	−26.3507	6.40598	−0.70330	−0.01549	0.013949	−0.00166	8.79E-05	−1.8E-06
ARMAS	10, G1	0.216276	4.35865	0.336721	−1.13914	0.779416	−0.27476	0.053265	−0.00574	0.000324	−7.5E-06
NAIRAS	11, G1	−21.2343	14.6438	14.9004	−15.4555	6.16156	−1.36743	0.182961	−0.01469	0.000654	−1.2E-05
ARMAS	11, G1	1.21628	4.35865	0.336721	−1.13914	0.779416	−0.27476	0.053265	−0.00574	0.000324	−7.5E-06
NAIRAS	12, G1	−4.15476	−27.8520	57.4237	−37.6847	13.0862	−2.72471	0.352203	−0.02774	0.001220	−2.3E-05
ARMAS	12, G1	2.21628	4.35865	0.336721	−1.13914	0.779416	−0.27476	0.053265	−0.00574	0.000324	−7.5E-06
NAIRAS	13, G1	16.2628	−73.0747	98.0349	−57.0201	18.6263	−3.73121	0.469278	−0.03620	0.001567	−2.9E-05
ARMAS	13, G1	3.21628	4.35865	0.336721	−1.13914	0.779416	−0.27476	0.053265	−0.00574	0.000324	−7.5E-06
NAIRAS	14, G1	36.0920	−117.392	137.988	−76.0618	24.0794	−4.72059	0.584189	−0.04449	0.001907	−3.5E-05
ARMAS	14, G1	4.21628	4.35865	0.336721	−1.13914	0.779416	−0.27476	0.053265	−0.00574	0.000324	−7.5E-06
NAIRAS	09, G2	−2.22734	−10.3078	24.9100	−16.6442	5.79795	−1.20744	0.156187	−0.01233	0.000545	−1.0E-05
ARMAS	09, G2	−2.38469	3.18807	3.67270	−4.71419	2.82626	−0.91023	0.165235	−0.01699	0.000926	−2.1E-05
NAIRAS	10, G2	0.968543	−21.7801	38.7883	−24.3867	8.26451	−1.69324	0.216620	−0.01696	0.000746	−1.4E-05
ARMAS	10, G2	−1.38469	3.18807	3.67270	−4.71419	2.82626	−0.91023	0.165235	−0.01699	0.000926	−2.1E-05
NAIRAS	11, G2	9.40559	−45.5540	64.3194	−38.0779	12.5588	−2.53301	0.320593	−0.02490	0.001087	−2.0E-05
ARMAS	11, G2	−0.38469	3.18807	3.67270	−4.71419	2.82626	−0.91023	0.165235	−0.01699	0.000926	−2.1E-05
NAIRAS	12, G2	27.1716	−90.4500	109.905	−62.2893	20.2113	−4.05178	0.511939	−0.03977	0.001737	−3.3E-05
ARMAS	12, G2	0.615307	3.18807	3.67270	−4.71419	2.82626	−0.91023	0.165235	−0.01699	0.000926	−2.1E-05
NAIRAS	13, G2	57.0443	−157.933	172.216	−93.1255	29.4205	−5.79495	0.722859	−0.05560	0.002409	−4.5E-05
ARMAS	13, G2	1.61531	3.18807	3.67270	−4.71419	2.82626	−0.91023	0.165235	−0.01699	0.000926	−2.1E-05
NAIRAS	14, G2	84.1934	−218.885	227.976	−120.414	37.4789	−7.30413	0.903685	−0.06905	0.002975	−5.5E-05
ARMAS	14, G2	2.61531	3.18807	3.67270	−4.71419	2.82626	−0.91023	0.165235	−0.01699	0.000926	−2.1E-05
NAIRAS	09, G3	−12.5287	6.73022	13.4399	−11.9904	4.54699	−0.98067	0.128920	−0.01025	0.000454	−8.6E-06
ARMAS	09, G3	−67.9924	55.9270	17.9864	−30.7064	13.4067	−3.04809	0.405152	−0.03171	0.001355	−2.4E-05
NAIRAS	10, G3	−9.48434	−6.67521	30.7706	−22.0122	7.81816	−1.63590	0.211324	−0.01661	0.000730	−1.4E-05
ARMAS	10, G3	−66.9924	55.9270	17.9864	−30.7064	13.4067	−3.04809	0.405152	−0.03171	0.001355	−2.4E-05
NAIRAS	11, G3	3.22622	−43.6991	71.3647	−44.3151	14.9702	−3.06105	0.390513	−0.03046	0.001331	−2.5E-05
ARMAS	11, G3	−65.9924	55.9270	17.9864	−30.7064	13.4067	−3.04809	0.405152	−0.03171	0.001355	−2.4E-05
NAIRAS	12, G3	19.3496	−88.3139	119.258	−70.5903	23.4445	−4.76424	0.606728	−0.04733	0.002070	−3.9E-05
ARMAS	12, G3	−64.9924	55.9270	17.9864	−30.7064	13.4067	−3.04809	0.405152	−0.03171	0.001355	−2.4E-05
NAIRAS	13, G3	56.3602	−175.769	203.079	−113.424	36.5942	−7.31263	0.921325	−0.07134	0.003104	−5.8E-05
ARMAS	13, G3	−63.9924	55.9270	17.9864	−30.7064	13.4067	−3.04809	0.405152	−0.03171	0.001355	−2.4E-05
NAIRAS	14, G3	98.7997	−275.114	297.676	−161.645	51.3967	−10.1856	1.27686	−0.09857	0.004280	−8.0E-05
ARMAS	14, G3	−62.9924	55.9270	17.9864	−30.7064	13.4067	−3.04809	0.405152	−0.03171	0.001355	−2.4E-05

Note. GCRs = galactic cosmic rays; NAIRAS = Nowcast of Atmospheric Ionizing Radiation for Aviation Safety; ARMAS = Automated Radiation Measurements for Aerospace Safety.

3. Discussion

Equations (2) and (3) represent a method for specifying the radiation environment at aviation altitudes for a global context, based on altitude, *L* shell, and geomagnetic activity. The ARMAS data are predominantly collected in the Western Hemisphere so we do not claim to have a global data set from which these equations were derived. However, because of the titled dipole of the Earth's main field, we have serendipitously been able to make a lot of observations across a wide range of magnetic latitudes since the field dips equatorward

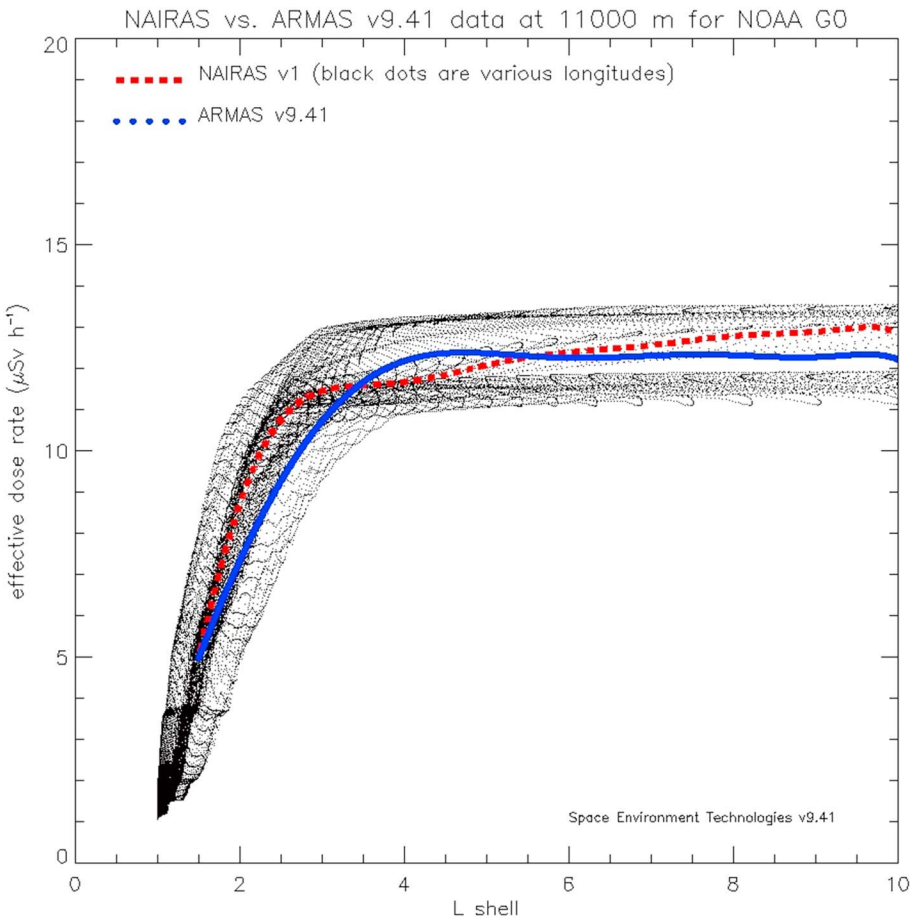

Figure 3. NAIRAS GCR climatology (red and black) and ARMAS statistical database (blue) effective dose rates for NOAA G0 geomagnetic conditions at 11 km using equation (2) coefficients from Table 2. NAIRAS = Nowcast of Atmospheric Ionizing Radiation for Aviation Safety; GCR = galactic cosmic ray; ARMAS = Automated Radiation Measurements for Aerospace Safety; NOAA = National Oceanic and Atmospheric Administration.

substantially in the American sector. This feature enables us to use a large number of observations across *L* shells from 1 to 7 to sample a globally representative range of cutoff rigidities and has enabled us to identify two types of environments during solar cycle 24 from moderate (2013) to minimum (2018). These are (i) the generalized global scale GCR-only environment in equation (2) for NAIRAS and ARMAS data and (ii) a GCR + probable REP subset environment using ARMAS data alone.

Previous empirical relationships have also been created such PCAIRE (McCall et al., 2009) and FDOSCalc (Wissmann et al., 2010) from mostly the GCR environment. While out of the scope of this paper, a comparative study of their results with the ARMAS database representations would certainly be a worthwhile exercise. For example, both PCAIRE and ARMAS equations were developed as mathematical models representing flight measurement databases. PCAIRE used the TEPC instrument for assembling its database and is driven by date/time and flight path. These inputs are correlated with GCR-related dose estimates based on the solar cycle, altitude, and magnetic latitudes/longitudes. SEP-related dose can be estimated with postevent analyses. ARMAS uses a different detector, the Teledyne micro dosimeter, where the measurements have been calibrated to the NASA RaD-X mission, which had an ensemble of instruments including TEPC, Liulin, and Teledyne micro dosimeters. The ARMAS equations provide both the GCR- and REP-related dose estimates but not those for SEPs, since none occurred during ARMAS measurement flights. Thus, a particularly useful future comparison would be between PCAIRE, ARMAS, and NAIRAS GCR-related dose estimates.

A unique feature of this work is the representation of the suggested REP contribution. As previously noted for the Liulin ISS measurements (Dachev, 2017; Dachev et al., 2017) relativistic electrons and/or bremsstrahlung

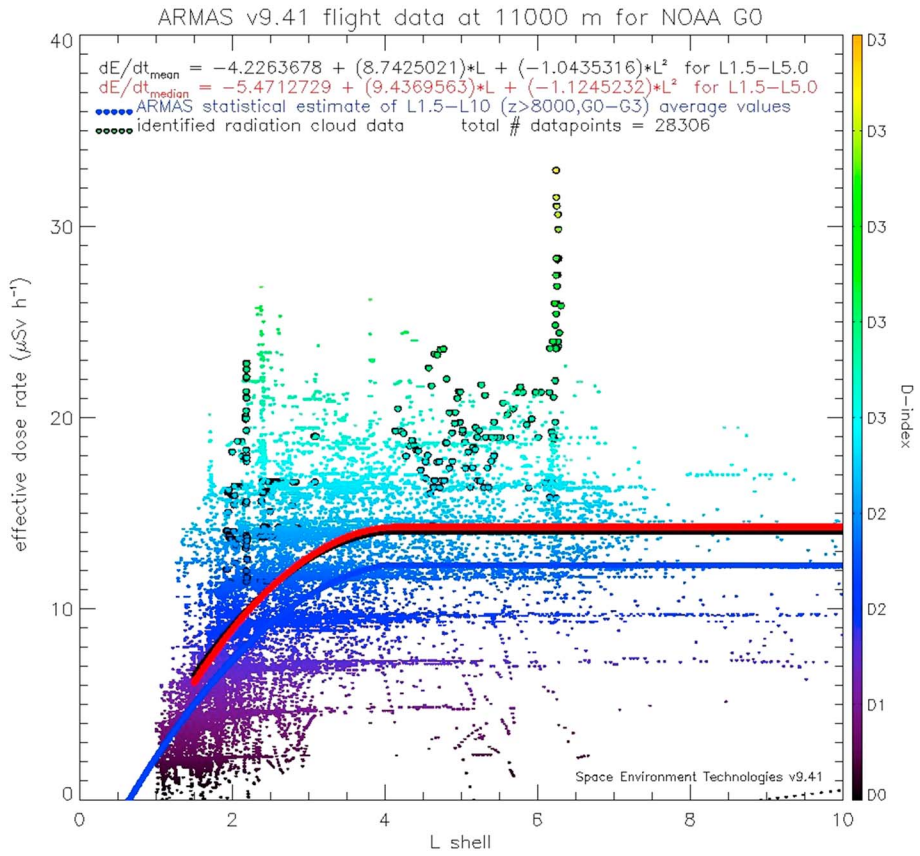

Figure 4. ARMAS effective dose rate GCR statistical background (black dotted line), median GCR + REP database (red), and mean GCR + REP database (black), for NOAA G0 geomagnetic conditions at 11 km using equation (3) coefficients from Table 3. ARMAS = Automated Radiation Measurements for Aerospace Safety; GCR = galactic cosmic ray; REP = relativistic energetic particle; NOAA = National Oceanic and Atmospheric Administration.

originating in the ORB have been seen on many occasions. ARMAS has also been able to collect a large number of observations in the Western Hemisphere at higher magnetic latitudes representing *L* shells between 1.5 and 5. These data are particularly abundant during quiet and minor geomagnetic disturbances including high-speed streams. While this work does not yet make a one-to-one correspondence between ISS Liulin and ARMAS observations, it is apparent from the data quantity of both instruments that this is an area ripe for further study. One objective of this paper is to make the ARMAS observations readily available to the scientific community so that comparisons may be made and so that the suggested radiation belt link to atmospheric radiation can be investigated further.

Table 3
ARMAS Effective Dose Rate Coefficients for Combined Median GCRs + Possible REPs

Database	*z*, *GX*	B_0	B_1	B_2
ARMAS	09, G0	−1.6563869	4.6659730	−0.54834584
ARMAS	10, G0	−1.3475229	5.2976860	−0.56838975
ARMAS	10, G1	−1.0346314	5.3443452	−0.63451370
ARMAS	11, G0	−2.8067264	7.4118563	−0.81062762
ARMAS	11, G1	−11.364783	14.007976	−1.7889658
ARMAS	12, G0	−1.3745376	7.7281473	−0.87191219
ARMAS	12, G1	0.99089356	6.2850045	−0.52568698
ARMAS	13, G0	−3.0994227	11.114310	−1.6098872

Note. ARMAS = Automated Radiation Measurements for Aerospace Safety; GCR = galactic cosmic ray; REP = relativistic energetic particle.

A particular feature of the ARMAS database is that measurements for *L* shells between 1.5 and 5 contain an additional contribution of radiation above the GCR background. These additional radiation levels have been carefully studied in over 50 cases and are not instrument artifacts whose characteristics have been previously described (Tobiska et al., 2016). A common characteristic of these enhanced radiation event periods is that the radiation levels during flight start at the GCR background level, rise to almost a factor of 2 higher, and then return to background GCR levels within less than an hour. This is consistent with flight through a secondary, Bremstrahlung γ ray beam. In Figure 4 we show some of these carefully studied events with an additional radiation component above the GCR background; these are highlighted as black circled dots. Throughout the

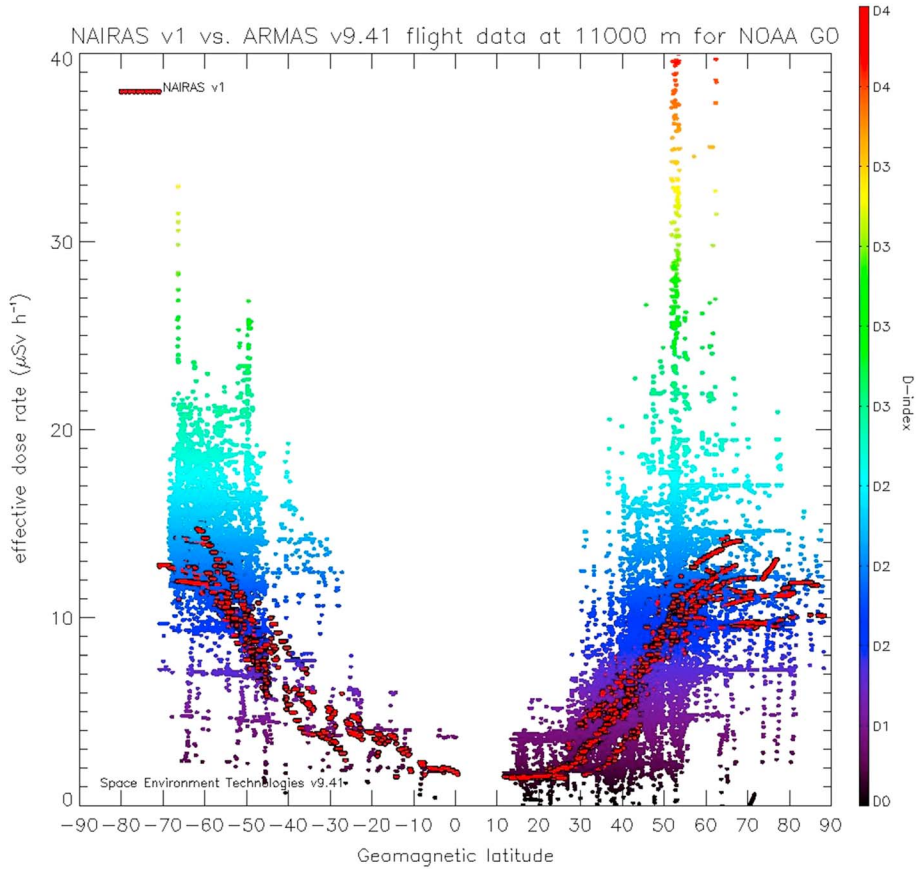

Figure 5. ARMAS derived effective dose rate (colored dots) compared with NAIRAS (red dots circled in black) for NOAA G0 geomagnetic conditions at 11 km for all geomagnetic latitudes. ARMAS = Automated Radiation Measurements for Aerospace Safety; NAIRAS = Nowcast of Atmospheric Ionizing Radiation for Aviation Safety; NOAA = National Oceanic and Atmospheric Administration.

ARMAS database, there have been nearly 100 cases of these types of enhanced radiation events that are candidates for study related to effects from radiation belt particles. Figure 5 shows an example of ARMAS measurements compared with NAIRAS for NOAA G0 conditions at 11 km across all geomagnetic latitudes. The NAIRAS climatology data generally represent the GCR median values in the ARMAS data, while the latter consistently show enhanced (or lower) dose rates for the higher geomagnetic latitudes with large variability. Equatorial values for NAIRAS and ARMAS are similar. Our study here suggests that the ensemble effects of these enhanced radiation events are statistically higher than the GCR background, that is, 15% higher near $L = 4$ (Figure 4 for G0 conditions at 11 km). For typical events such as the 3 October 2015 flight, for example, the ratio of the combined GCR plus possible REP data to GCR only at L shell = 4 is 1.32.

4. Applications for Equations Representing the Databases

4.1. Radiation Environment Climatology Baseline

The radiation databases for NAIRAS climatology and ARMAS statistical weather are represented by equations (2) and (3), respectively, using the equation coefficients in Tables 2 and 3. These two databases represent an accurate estimate of derived effective dose rates for all locations around the planet from moderate activity in solar cycle 24 (2013) to the minimum of solar cycle 24 (2018). For very low L shells in equatorial regions, that is, $1.0 \leq L < 1.5$, the effective dose rates are nearly identical to those for $L = 1.5$ and they can be set to the $L = 1.5$ values; for very high L shells in polar regions, the effective dose rates are nearly identical to those for $L = 5$ and they can be set to the $L = 5$ values. Since GCRs account for most of the source particles across all L shells, we suggest that an effective dose rate climatological baseline is the rate represented by

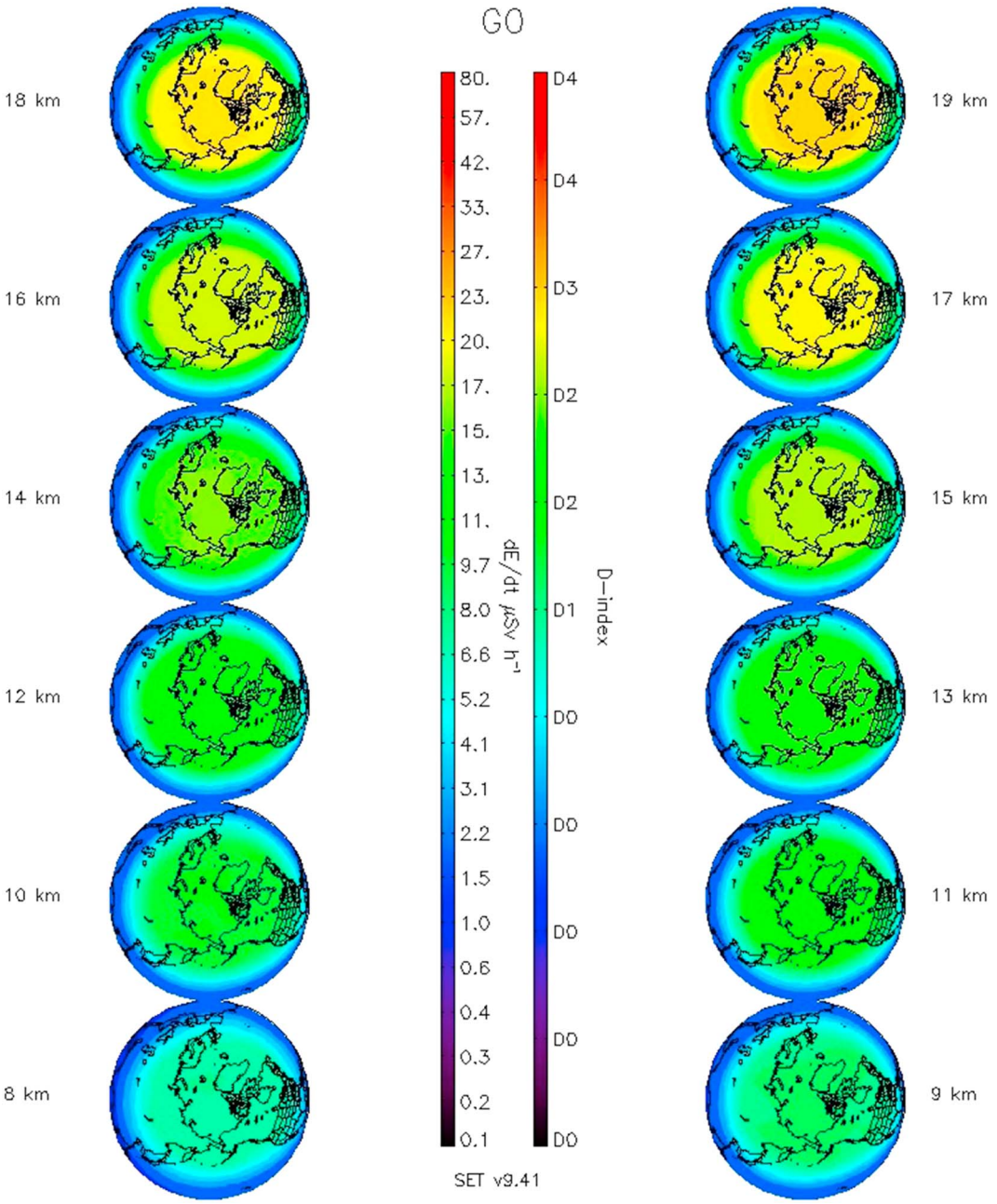

Figure 6. Climatological forecast for galactic cosmic rays only of the effective dose rates, d*E*/d*t*, from 8 to 19 km based on the Nowcast of Atmospheric Ionizing Radiation for Aviation Safety model for the National Oceanic and Atmospheric Administration G-scale geomagnetic conditions of G0.

equation (2) using the Table 2 NAIRAS coefficients. These are based on the polynomial fit of the NAIRAS global data as a function of altitude, *L* shell, and geomagnetic activity. The NAIRAS model data can be considered validated by ARMAS as demonstrated by comparing equation (2) and Table 2 ARMAS coefficients results, particularly as plotted in the supporting information. In Figure 3 the small black dots are the range of NAIRAS GCR climatological variability across all magnetic longitudes.

In a narrow band of *L* shell values for both Northern and Southern Hemispheres, that is, $1.5 \leq L \leq 5.0$, we suggest that a baseline for effective dose rates representative of GCR climatology plus probable REP statistical weather can be characterized using equation (3) and Table 3 ARMAS coefficients; these are based on the polynomial fit of the statistical median of the ARMAS data alone as a function of altitude, *L* shell, and

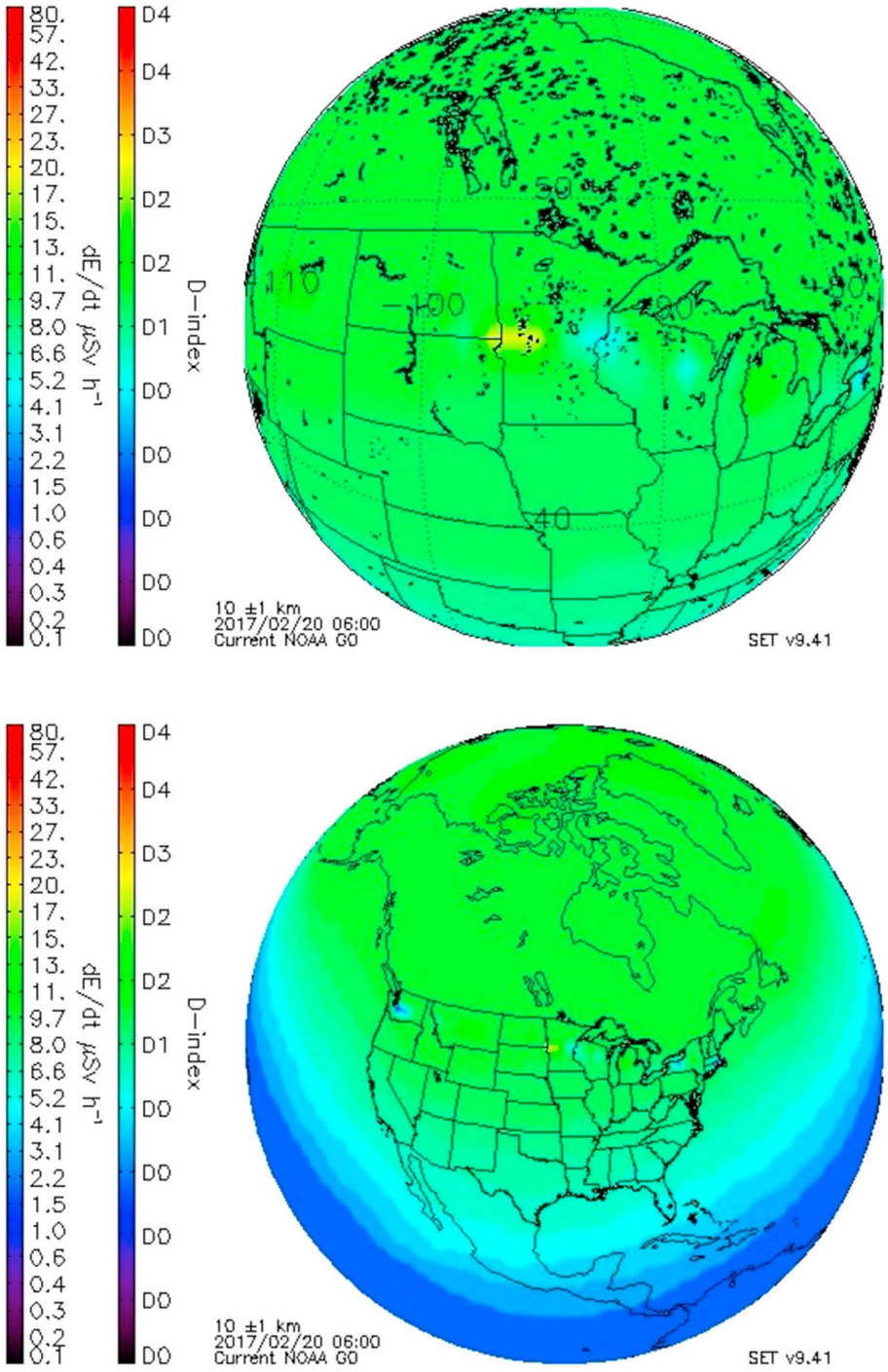

Figure 7. (top) Regional and airport nowcast effective dose rate, d*E*/d*t*, showing the Continental U.S. (CONUS) air traffic control perspective between Boston and Seattle. (bottom) The aircraft route nowcast from Boston to Seattle. Both panels have a flight track with derived d*E*/d*t* on a commercial carrier at 10 km for 20 February 2017 overlaid on the nowcast.

geomagnetic activity. In Figure 4 the range of ARMAS GCR climatological (heavy blue line) plus REP weather variability (colored dots) is evident around the polynomial fit.

4.2. Climatological Forecasting

As a start toward hemispheric climatological and statistical weather forecasting, we provide examples in Figure 6 (Figures 6a–6e in supporting information) showing the Northern Hemisphere for geomagnetic

conditions of G0 (through G4 in supporting information) at 12 altitude layers (8–19 km in 1-km steps). These representations are plotted from the NAIRAS database. These are considered applicable to both nowcasting (current epoch) and forecasting (beyond current epoch). Forecasting is possible because the deterministic altitude and *L* shell position can be identified for a given flight path plus operationally predicted (forecast) geomagnetic activity levels are available.

The Figure 6 visual interpretation includes the *D*-index color scale alongside the effective dose rate and makes it very easy for pilots as well as air traffic management to assess near-term or future radiation safety hazards. Space Environment Technologies (SET) already continuously forecast the hourly geomagnetic conditions for *Dst* using two independent methods: its Anemomilos algorithm (Tobiska et al., 2013) and the NOAA Space Weather Prediction Center ENLIL model plus Rice University *Dst* neural net algorithm. The results of both algorithms' predictions are available at https://sol.spacenvironment.net/~sam_ops/index.html. Space Environment Technologies' operational system transforms the hourly *Dst* into a NOAA G-scale value, and this is used for creating the climatology forecast of the GCR radiation environment shown in Figure 6. Current operational forecasting for commercial and government customers is done with a 1-hr time granularity out to 144 hr (6 days) into the future.

4.3. Nowcasting and Alerts for Regions, Airports, and Routes

An example of how nowcasts might be applied to regions, airports, and individual aircraft routes is shown in Figure 7. Both the d*E*/d*t* effective dose rate and the *D*-index are shown in these examples for a commercial carrier aircraft at 10 km on 20 February 2017 flying from Boston to Seattle under G0 (quiet) geomagnetic conditions. The effective dose rate derived from measurements on the aircraft was about the same as the nowcast values for that flight (green). An advantage of this type of nowcast data product is that regional air traffic management centers, local international airports, and aircraft operations can all benefit from situational awareness products using GCR-induced effective dose rate estimates.

5. Conclusions

NAIRAS climatological and ARMAS statistical weather databases are represented in the form of polynomial fit equations. The global equations are based on altitude (9–14 km), *L* shell ($1.5 \leq L \leq 10$), and geomagnetic conditions (G0–G3) to provide estimated effective dose rates for any location on the planet. Both the NAIRAS and ARMAS databases represented by equation (2) using Table 2 coefficients are a result of the GCR-induced environment alone. There are no SEPs that have been observed so far in ARMAS. A subset of the ARMAS database is represented by a separate polynomial fit equation for the GCR + probable REP-enhanced effective dose rates in a narrow band of *L* shells ($2 \leq L \leq 5$) with an altitudinal (9–13 km) and geomagnetic (G0–G1) dependency shown by equation (3) using Table 3 coefficients. We also summarize a method to calculate the *D*-index for effective dose rate based on all sources of radiation as a decision aid tool for air traffic management and aircraft operations.

A unique feature of this work is the representation of a suggested REP contribution to an enhanced dose environment. It is heuristically supported by abundant Liulin ISS measurements of relativistic electrons and/or bremsstrahlung originating in the ORB that may have an effect at aviation altitudes in the form of bremsstrahlung γ rays. The ARMAS database for *L* shells between 1.5 and 5 clearly shows an additional contribution of radiation above the GCR background as shown in Figures 4 and 5. Throughout the ARMAS database, there are nearly 100 cases of these types of enhanced radiation events that are candidates for study related to effects from radiation belt particles. Our study here suggests that the ensemble effects of these enhanced radiation events are 15% higher than the GCR background at $L = 4$ for G0 conditions at 11 km.

There are useful applications for these databases. First, radiation climatology can be created to compare with measured weather variability. If measurements are not available, then the equations representing the NAIRAS and ARMAS databases enable climatological and statistical weather forecasting, respectively, if the flight path and forecast geomagnetic activity are known. Particularly noteworthy applications are for specifying the radiation environment relevant to regional air traffic management, to airport overflight operations, and to air carrier route operations for individual aircraft. The business jet community will find utility for flight path planning in the ARMAS and NAIRAS databases since they typically fly at higher altitudes than commercial aircraft and are susceptible to substantially greater radiation hazards.

Acknowledgments

The authors thank the reviewers for their timely and insightful comments that have improved this paper. The authors acknowledge the financial support for ARMAS from NASA NAIRAS DECISION project contract NNL07AA00C, NASA SBIR Phase I and Phase II program contracts NNX11CH03P and NNX12CA78C, NASA AFRC Phase III contracts NND14SA64P and NND15SA55C, the NASA LWS RADIAN project 80NSSC18K0187, the NASA FO ARMAS-Hi project NND17AP04A, the NASA SBIR ARMAS-DM project 80NSSC18P2111, and South Korean Space Weather Center matching funds for the ARMAS SBIR Phase IIE. The NASA Airborne Sciences Program and Armstrong Flight Research Center DC-8, ER-2, SOFIA, and Gulfstream 3 have provided welcome flight support for ARMAS instruments. E. Teets, S. Wiley, T. Moes, and R. Albertson have enabled successful measurements from AFRC, while L. Guhathakurta of NASA programmatically contributed to the successful G-3 observations. NOAA Space Weather Prediction Center used their good offices to facilitate ARMAS use on the NOAA Gulfstream 4, as did the National Center for Atmospheric Research High Altitude Observatory for ARMAS use on the National Science Foundation Gulfstream 5 and the Federal Aviation Administration's William J. Hughes Technical Center (WJHTC) for ARMAS use on the Bombardier Global 5000. The University of Alaska, Fairbanks, Geophysical Institute, provided welcome collaboration for obtaining ARMAS FM5 data on commercial flights across North America and the Korean Space Weather Center provided useful collaboration for ARMAS FM5 and FM6 flight data on commercial flights at higher latitudes across the North Pacific and in East Asia. The ARMAS archival data are publicly available at http://sol.spacenvironment.net/armas_ops/Archive/ and NAIRAS data at http://sol.spacenvironment.net/raps_ops/current_files/globeView.html.

References

Blake, J. B., Looper, M. D., Baker, D. N., Nakamura, R., Klecker, B., & Hovestadt, D. (1996). New high temporal and spatial resolution measurements by SAMPEX of the precipitation of relativistic electrons. *Advances in Space Research*, *18*(8), 171–186.

Carlson, P., & Watson, A. A. (2014). Erich Regener and the ionisation maximum of the atmosphere. *History of Geo- and Space Science*, *5*(2), 175–182.

Dachev, T. P. (2017). Relativistic electron precipitation bands in the outside radiation environment of the international space station. *Journal of Atmospheric and Solar-Terrestrial Physics*, *177*, 247–256. https://doi.org/10.1016/j.jastp.2017.11.008

Dachev, T. P., Bankov, N. G., Tomov, B. T., Matviichuk, Y. N., Dimitrov, P. G., Häder, D.-P., & Horneck, G. (2017). Overview of the ISS radiation environment observed during the ESA EXPOSE-R2 mission in 2014–2016. *Space Weather*, *15*, 1475–1489. https://doi.org/10.1002/2016SW001580

Dachev, T. P., Semkova, J. V., Tomov, B. T., Matviichuk, Y. N., Dimitrov, P. G., Koleva, R. T., et al. (2015). Overview of the Liulin type instruments for space radiation measurement and their scientific results. *Life Sciences and Space Research*, *4*, 92–114. https://doi.org/10.1016/j.lssr.2015.01.005

Dyer, C., Hands, A., Lei, F., Truscott, P., Ryden, K. A., Morris, P., et al. (2009). Advances in measuring and modeling the atmospheric radiation environment. *IEEE Transactions on Nuclear Science*, *56*(6), 3415–3422.

Dyer, C., & Lei, F. (2001). Monte-Carlo calculations of the influence on aircraft radiation environments of structures and solar particle events. *IEEE Transactions on Nuclear Science*, *48*(6), 1987–1995.

Dyer, C., Lei, F., Hands, A., Clucas, S., & Jones, B. (2005). Measurements of the atmospheric radiation environment from CREAM and comparisons with models for quiet time and solar particle events. *IEEE Transactions on Nuclear Science*, *52*(6), 2326–2331.

Dyer, C. S., Lei, F., Clucas, S. N., Smart, D. F., & Shea, M. A. (2003a). Solar particle enhancements of single event effect rates at aircraft altitudes. *IEEE Transactions on Nuclear Science*, *50*(6), 2038–2045.

Dyer, C. S., Lei, F., Clucas, S. N., Smart, D. F., & Shea, M. A. (2003b). Calculations and observations of solar particle enhancements to the radiation environment at aircraft altitudes. *Advances in Space Research*, *32*(1), 81–93.

Dyer, C. S., & Truscott, P. (1999). Cosmic radiation effects on avionics. *Radiation Protection Dosimetry*, *86*(4), 337–342.

Executive Order 13744 (2016). The white house, executive order—Coordinating efforts to prepare the nation for space weather events, October 13, 2016.

Federico, C. A., Gonçalez, O. L., Caldas, L. V. E., Pazianotto, M. T., Dyer, C., Caresana, M., & Hands, A. (2015). Radiation measurements onboard aircraft in the South Atlantic region. *Radiation Measurements*, *82*, 14e20–14e20. https://doi.org/10.1016/j.radmeas.2015.07.008

Getley, I. L., Bennett, L. G. I., Lewis, B. J., Bennett, B., Dyer, C. S., Hands, A. D. P., & Duldig, M. L. (2010). Evaluation of new cosmic radiation monitors designed for aircrew exposure assessment. *Space Weather*, *8*, S01001. https://doi.org/10.1029/2009SW000492

Gopalswamy, N. (2004). A global picture of CMEs in the inner heliosphere. In G. Poletto & S. Suess (Eds.), *The Sun and the heliosphere as an integrated system*, *ASSL series* (Vol. 317, pp. 201–251). Dordrecht, Netherlands: Springer.

Grajewski, B., Waters, M. A., Yong, L. C., Tseng, C.-Y., Zivkovich, Z., & Cassinelli, R. T. (2011). Airline pilot cosmic radiation and circadian disruption exposure assessment from logbooks and company records. *The Annals of Occupational Hygiene*, *55*(5), 465–475.

International Commission on Radiation Units (2010). *International commission on radiation units and measurements, reference data for the validation of doses from cosmic-radiation exposure of aircraft crew*, ICRU report 84, *J. ICRU* (Vol. 10). Oxford, UK: Oxford Univ. Press.

Iles, R. H. A., Jones, J. B. L., Taylor, G. C., Blake, J. B., Bentley, R. D., Hunter, R., et al. (2004). Effect of solar energetic particle (SEP) events on the radiation exposure levels to aircraft passengers and crew: Case study of 14 July 2000 SEP event. *Journal of Geophysical Research*, *109*, A11103. https://doi.org/10.1029/2003JA010343

International Agency for Research on Cancer (2000). Ionizing radiation, part 1, X- and γ-radiation and neutrons. In *IARC work. Group eval. Carcinog. risks hum* (Chapter 4, p. 75). France: IARC and World Health Organization, Lyon.

ICRP (2007). The 2007 Recommendations of the International Commission on Radiological Protection. ICRP Publication 103. *Ann ICRP*, *37*(2–4), 1–332.

International Electrotechnical Commission (IEC) 62396-1 (2012). Process management for avionics - Atmospheric radiation effects - Part 1: Accommodation of atmospheric radiation effects via single event effects within avionics electronic equipment (Edition 1.0).

Lee, J., Nam, U.-W., Pyo, J., Kim, S., Kwon, Y.-J., Lee, J., et al. (2015). Short-term variation of cosmic radiation measured by aircraft under constant flight conditions. *Space Weather*, *13*, 797–806. https://doi.org/10.1002/2015SW001288

McCall, M. J., Lemay, F., Bean, M. R., Lewis, B. J., & Bennett, L. G. (2009). Development of a predictive code for aircrew radiation exposure. *Radiation Protection Dosimetry*, *136*(4), 274–281. https://doi.org/10.1093/rpd/ncp130

McIlwain, C. E. (1961). Coordinates for mapping the distribution of magnetically trapped particles. *Journal of Geophysical Research*, *66*(11), 3681–3691. https://doi.org/10.1029/JZ066i011p03681

Meier, M. M., Hubiak, M., Matthiae, D., Wirtz, M., & Reitz, G. (2009). Dosimetry at aviation altitudes (2006–2008). *Radiation Protection Dosimetry*, *136*(4), 251–255.

Meier, M. M., Matthiä, D., Forkert, T., Wirtz, M., Scheibinger, M., Hübel, R., & Mertens, C. J. (2016). RaD-X: Complementary measurements of dose rates at aviation altitudes. *Space Weather*, *14*, 689–694. https://doi.org/10.1002/2016SW001418

Meier, M. M., & Matthiae, D. D. (2014). A space weather index for the radiation field at aviation altitudes. *Journal of Space Weather and Space Climate*, *4*, A13.

Meier, M. M., Trompier, F., Ambrozova, I., Kubancak, J., Matthiae, D., Ploc, O., et al. (2016). CONCORD: Comparison of cosmic radiation detectors in the radiation field at aviation altitudes. *Journal of Space Weather and Space Climate*, *6*, A24. https://doi.org/10.1051/swsc/2016017

Mertens, C. J. (2016). Overview of the radiation dosimetry experiment (RaD-X) flight mission. *Space Weather*, *14*, 874–898. https://doi.org/10.1002/2016SW001407

Mertens, C. J., Gronoff, G. P., Norman, R. B., Hayes, B. M., Lusby, T. C., Straume, T., et al. (2016). Cosmic radiation dose measurements from the RaD-X flight campaign. *Space Weather*, *14*, 874–898. https://doi.org/10.1002/2016SW001407

Mertens, C. J., Meier, M. M., Brown, S., Norman, R. B., & Xu, X. (2013). NAIRAS aircraft radiation model development, dose climatology, and initial validation. *Space Weather*, *11*, 603–635. https://doi.org/10.1002/swe.20100

Morley, S. K., Brito, T. V., & Welling, D. T. (2018). Measures of model performance based on the log accuracy ratio. *Space Weather*, *16*, 69–88. https://doi.org/10.1002/2017SW001669

Mutuel, L. H. (2016). Single event effects mitigation techniques report, Department of Transportation/Federal Aviation Administration, TC-15/62, February 2016.

National Science and Technology Council (2015). National Space Weather Action Plan, October 2015.

Norman, R. B., Mertens, C. J., & Slaba, T. C. (2016). Evaluating galactic cosmic ray environment models using RaD-X flight data. *Space Weather*, *14*, 764–775. https://doi.org/10.1002/2016SW001401

Normand, E., Oberg, D. L., Wert, J. L., Ness, J. D., Majewski, P. P., Wender, S., & Gavron, A. (1994). Single event upset and charge collection measurements using high energy protons and neutrons. *IEEE Transactions on Nuclear Science*, *41*(6), 2203–2209.

Normand, E., Vranish, K., Sheets, A., Stitt, M., & Kim, R. (2006). Quantifying the double-sided neutron SEU threat, from low energy (thermal) and high energy (>10 MeV) neutrons. *IEEE Transactions on Nuclear Science*, *53*(6), 3587–3595.

Ploc, O., Ambrozova, I., Kubancak, J., Kovar, I., & Dachev, T. P. (2013). Publicly available database of measurements with the silicon spectrometer Liulin onboard aircraft. *Radiation Measurements*, *58*, 107–112. https://doi.org/10.1016/j.radmeas.2013.09.002

Ploc, O., Pachnerova Brabcova, K., Spurny, F., Malusek, A., & Dachev, T. (2011). Use of energy deposition spectrometer Liulin for individual monitoring of aircrew. *Radiation Protection Dosimetry*, *144*, 611e614.

Reames, D. V. (2013). The two sources of solar energetic particles. *Space Science Reviews*, *175*(1-4), 53–92. https://doi.org/10.1007/s11214-013-9958-9

Regener, E., & Pfotzer, G. (1935). Vertical intensity of cosmic rays by threefold coincidences in the stratosphere. *Nature*, *136*(3444), 718–719.

Shea, M. A., Smart, D. F., & Gentile, L. C. (1987). Estimating cosmic ray vertical cutoff rigidities as a function of the McIlwain L-parameter for different epochs of the geomagnetic field. *Physics of the Earth and Planetary Interiors*, *48*(3-4), 200–205.

Simpson, J. A. (1983). Elemental and isotopic composition of the galactic cosmic rays. *Annual Review of Nuclear and Particle Science*, *33*(1), 323–382. https://doi.org/10.1146/annurev.ns.33.120183.001543

Smart, D. F., & Shea, M. A. (1967). A study of the effectiveness of the McIlwain coordinates in estimating cosmic-ray vertical cutoff rigidities. *Journal of Geophysical Research*, *72*(13), 3447–3454.

Spurny, F., & Dachev, T. (2001). Measurements during an intense solar flare, GLE 60. *Radiation Protection Dosimetry*, *95*, 273e275.

Spurny, F., & Dachev, T. (2002). On board aircrew dosimetry with a semiconductor spectrometer. *Radiation Protection Dosimetry*, *100*, 525e528.

Tobiska, W. K., Atwell, W., Beck, P., Benton, E., Copeland, K., Dyer, C., et al. (2015). Advances in atmospheric radiation measurements and modeling needed to improve air safety. *Space Weather*, *13*, 202–210. https://doi.org/10.1002/2015SW001169

Tobiska, W. K., Bouwer, D., Smart, D., Shea, M., Bailey, J., Didkovsky, L., et al. (2016). Global real-time dose measurements using the Automated Radiation Measurements for Aerospace Safety (ARMAS) system. *Space Weather*, *14*, 1053–1080. https://doi.org/10.1002/2016SW001419

Tobiska, W. K., Knipp, D., Burke, W. J., Bouwer, D., Bailey, J., Odstrcil, D., et al. (2013). The Anemomilos prediction methodology for Dst. *Space Weather*, *11*, 490–508. https://doi.org/10.1002/swe.20094

Tobiska, W. K., Meier, M. M., Matthiae, D., & Copeland, K. (2017). Characterizing the variation in atmospheric radiation at aviation altitudes. In N. Buzulukova (Ed.), *Extreme events in geospace* (pp. 453–471). Cambridge, MA: Elsevier.

United Nations Scientific Committee on the Effect of Atomic Radiation (2000). Sources and effect of ionizing radiation, United Nations Scientific Committee on the Effect of Atomic Radiation UNSCEAR 2000 Report to the General Assembly, with Scientific Annexes, Vol. II, Annex G.

Wissmann, F., Reginatto, M., & Möller, T. (2010). Ambient dose equivalent at flight altitudes: A fit to a large set of data using a Bayesian approach. *Journal of Radiological Protection*, *30*(3), 513–524.